

SPATIO-TEMPORAL VIDEO AUTOENCODER WITH DIFFERENTIABLE MEMORY

Viorica Pătrăucean, Ankur Handa & Roberto Cipolla

Department of Engineering

University of Cambridge, UK

{vp344, ah781, rc10001}@cam.ac.uk

ABSTRACT

We describe a new spatio-temporal video autoencoder, based on a classic spatial image autoencoder and a novel nested temporal autoencoder. The temporal encoder is represented by a differentiable visual memory composed of convolutional long short-term memory (LSTM) cells that integrate changes over time. Here we target motion changes and use as temporal decoder a robust optical flow prediction module together with an image sampler serving as built-in feedback loop. The architecture is end-to-end differentiable. At each time step, the system receives as input a video frame, predicts the optical flow based on the current observation and the LSTM memory state as a dense transformation map, and applies it to the current frame to generate the next frame. By minimising the reconstruction error between the predicted next frame and the corresponding ground truth next frame, we train the whole system to extract features useful for motion estimation without any supervision effort. We believe these features can in turn facilitate learning high-level tasks such as path planning, semantic segmentation, or action recognition, reducing the overall supervision effort.

1 INTRODUCTION

High-level understanding of video sequences is crucial for any autonomous intelligent agent, *e.g.* semantic segmentation is indispensable for navigation, or object detection skills condition any form of interaction with objects in a scene. The recent success of convolutional neural networks in tackling these high-level tasks for static images opens up the path for numerous applications. However, transferring the capabilities of these systems to tasks involving video sequences is not trivial, on the one hand due to the lack of video labelled data, and on the other hand due to convnets' inability of exploiting temporal redundancy present in videos. Motivated by these two shortcomings, we focus on reducing the supervision effort required to train recurrent neural networks, which are known for their ability to handle sequential input data (Williams & Zipser, 1995; Hochreiter et al., 2000).

In particular, we describe a spatio-temporal video autoencoder integrating a differentiable short-term memory module whose (unsupervised) training is geared towards motion estimation and prediction (Horn & Schunck, 1994). This choice has biological inspiration. The human brain has a complex system of visual memory modules, including visual short-term memory (VSTM), iconic memory, and long-term memory (Hollingworth, 2004). Among them, VSTM is responsible mainly for understanding visual changes (movement, light changes) in dynamic environments, by integrating visual stimuli over periods of time (Phillips, 1974; Magnussen, 2000). Moreover, the fact that infants are able to handle occlusion, containment, and covering events by the age of 2.5 months (Baillargeon, 2004) could suggest that the primary skills acquired by VSTM are related to extracting features useful for motion understanding. These features in turn could generate objectness awareness based on the simple principle that points moving together belong to the same object. Understanding objectness is crucial for high-level tasks such as semantic segmentation or action recognition (Alexe et al., 2012). In this spirit, our approach is similar to the recent work of Agrawal et al. (2015), who show that the features learnt by exploiting (freely-available) ego-motion information as supervision data are as good as features extracted with human-labelled supervision data. We believe that our work is complementary to their approach and integrating them could lead to an artificial agent with enhanced vision capabilities.

Our implementation draws inspiration from standard video encoders and compression schemes, and suggests that deep video autoencoders should differ conceptually from spatial image autoencoders. A video autoencoder need not reproduce *by heart* an entire video sequence. Instead, it should be able to encode the significant differences that would allow it to reconstruct a frame given a previous frame. To this end, we use a classic convolutional image encoder – decoder with a nested memory module composed of convolutional LSTM cells, acting as temporal encoder. Since we focus on learning features for motion prediction, we use as temporal decoder a robust optical flow prediction module together with an image sampler, which provides immediate feedback on the predicted flow map. At each time step, the system receives as input a video frame, predicts the optical flow based on the current frame and the LSTM content as a dense transformation map, and applies it to the current frame to predict the next frame. By minimising the reconstruction error between the predicted next frame and the ground truth next frame, we are able to train the whole system for motion prediction with no supervision effort. Other modules handling other types of variations like light changes could be added in parallel, inspired by neuroscience findings which suggest that VSTM is composed of a series of different modules specialised in handling the low-level processes triggered by visual changes, all of them connected to a shared memory module (Magnussen, 2000). Note that at the hardware level, this variations-centred reasoning is similar to event-based cameras (Boahen, 2005), which have started to make an impact in robotic applications (Kim et al., 2014).

Our contribution resides at the experimental level. We propose a spatio-temporal version of LSTM cells to serve as a basic form of visual short-term memory (temporal encoder), and make available an end-to-end differentiable architecture with built-in feedback loop, that allows effortless training and experimentation with the goal of understanding the role of such an artificial visual short-term memory in low-level visual processes and its implications in high-level visual tasks. All our code (Torch implementation) is available online (Con).

2 RELATED WORK

Architectures based on LSTM cells (Hochreiter & Schmidhuber, 1997) have been very successful in various tasks involving one-dimensional temporal sequences: speech recognition (Sak et al., 2014), machine translation (Sutskever et al., 2014), music composition (Eck & Schmidhuber), due to their ability to preserve information over long periods of time. Multi-dimensional LSTM networks have been proposed to deal with (2D) images (Graves et al., 2007) or (3D) volumetric data (Stollenga et al., 2015), treating the data as spatial sequences. Since in our work we aim at building a visual short-term memory, customised LSTM cells that deal with temporal sequences of spatial data represent a natural choice.

Recently, Srivastava et al. (2015) proposed an LSTM-based video autoencoder, which aims at generating past and future frames in a sequence, in an unsupervised manner. However, their LSTM implementation treats the input as linear sequences by linearising the frames or by using 1D frame representations produced after the last fully-connected layer of a convolutional neural network. This results in a large number of parameters, since the activations of the LSTM cells use fully-connected multiplicative operations, which are not necessarily useful for 2D images, since natural image statistics indicate only local correlations. Another difference is in the architecture setup. We are not interested in training a black-box to produce past and future frames in the sequence. Instead we aim at a transparent setup, and train a more generic memory module together with specialised modules able to decode the memory content and on which appropriate constraints (sparsity, smoothness) can be imposed.

Our approach is partially related to optical flow estimation works like DeepFlow (Weinzaepfel et al., 2013) and FlowNet (Fischer et al., 2015). However, these methods use purely supervised training to establish matches between consecutive pairs of frames in a sequence, and then apply a variational smoothing. Our architecture is end-to-end differentiable and integrates a smoothness penalty (Huber penalty) to ensure that nearby pixels follow a locally smooth motion, and requires no labelled training data.

As mentioned in the previous section, our work is similar in spirit to (Agrawal et al., 2015), by establishing a direct link between vision and motion, in an attempt to reduce supervision effort for high-level scene understanding tasks. However, instead of relying on IMU input from which we can only estimate a global transformation representing the ego-motion, we predict a dense flow map by

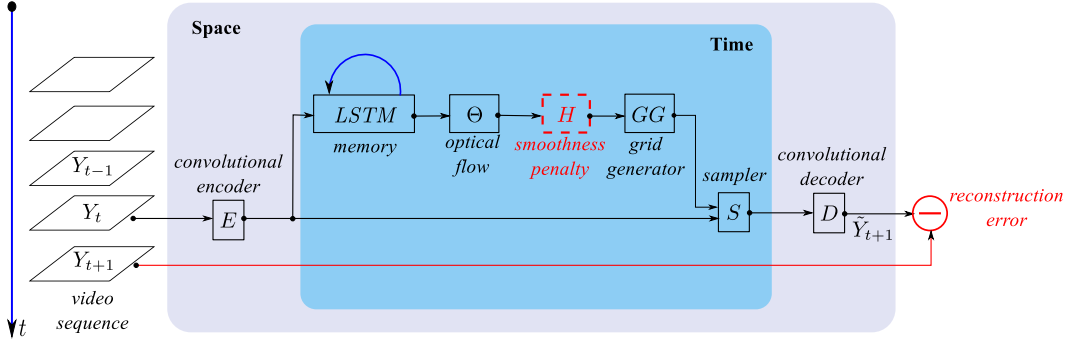
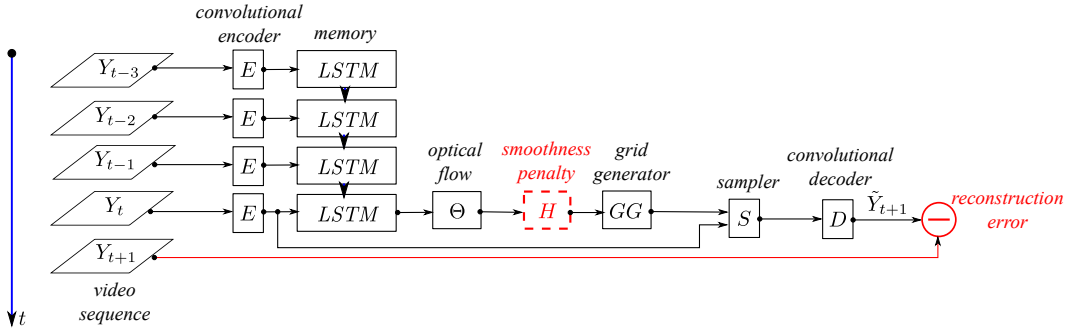


Figure 1: Spatio-temporal video autoencoder.

Figure 2: Unfolding of the architecture for $\tau = 4$ time steps. Only the output from the last time step is used in optimisation. Note that the encoder module preceding the memory module needs to be unfolded as well, even if it is not recurrent, to ensure that the gradients are backpropagated correctly.

integrating visual stimuli over time using a memory module, and then we use a built-in feedback loop to assess the prediction. The dense flow map is useful to explain dynamic environments, where different objects can follow different motion models, hence a global transformation is not sufficient (Menze & Geiger, 2015).

3 ARCHITECTURE

Our architecture consists of a temporal autoencoder nested into a spatial autoencoder (see Figure 1). At each time step, the network takes as input a video frame Y_t of size $H \times W$, and generates an output of the same size, representing the predicted next frame, \tilde{Y}_{t+1} . In the following, we describe each of the modules in detail.

3.1 SPATIAL AUTOENCODER E AND D

The spatial autoencoder is a classic convolutional encoder – decoder architecture. The encoder E contains a convolutional layer, followed by tanh non-linearity and a spatial max-pooling with subsampling layer. The decoder D mirrors the encoder, except for the non-linearity layer, and uses nearest-neighbour spatial upsampling to bring the output back to the size of the original input. After the forward pass through the spatial encoder $Y_t \xrightarrow{E} x_t$, the size of the feature maps x_t is $d \times h \times w$, d being the number of features, and h and w the height and width after downsampling, respectively.

3.2 TEMPORAL AUTOENCODER

The goal of the temporal autoencoder is to capture significant changes due to motion (ego-motion or movement of the objects in the scene), that would allow it to predict the visual future, knowing

the past and the present. In a classic spatial autoencoder (Masci et al., 2011), the encoder and decoder learn proprietary feature spaces that allow an optimal decomposition of the input using some form of regularisation to prevent learning a trivial mapping. The encoder decides freely upon a decomposition based on its current feature space, and the decoder constrains the learning of its own feature space to satisfy this decomposition and to reconstruct the input, using usually operations very similar to the encoder, and having the same number of degrees of freedom. Differently from this, the proposed temporal autoencoder has a decoder with a small number of trainable parameters, whose role is mainly to provide immediate feedback to the encoder, but without the capacity of amending encoder’s mistakes like in the spatial case. In optimisation terms, the error during learning is attributed mainly to the encoder, which is now more constrained to produce sensible feature maps.

3.2.1 MEMORY MODULE *LSTM*

The core of the proposed architecture is the memory module playing the role of a temporal encoder. We aim at building a basic visual short-term memory, which preserves locality and layout ensuring a fast access and bypassing more complicated addressing mechanisms like those used by neural Turing machines (Graves et al., 2014). To this end, we use customised spatio-temporal LSTM cells with the same layout as the input. At each time step t , the *LSTM* module receives as input a new video frame after projection in the spatial feature space. This is used together with the memory content and output of the previous step $t - 1$ to compute the new memory activations. This operation can be easily understood by unfolding the recurrent module over a number of time steps (see Figure 2).

Classic LSTM cells operate over sequences of linear inputs and perform biased linear (fully-connected) multiplications, followed by non-linearities to compute gate and cell activations. In our case, to deal with the spatial and local nature of the video frames, we replace the linear multiplication operation with spatial local convolutions.

All-in-all, the activations of a spatio-temporal convolutional LSTM cell at time t are given by:

$$\begin{cases} i_t &= \sigma(x_t * w_{xi} + h_{t-1} * w_{hi} + w_{ibias}) \\ f_t &= \sigma(x_t * w_{xf} + h_{t-1} * w_{hf} + w_{fbias}) \\ \tilde{c}_t &= \tanh(x_t * w_{xc} + h_{t-1} * w_{hc} + w_{cbias}) \\ c_t &= \tilde{c}_t \odot i_t + c_{t-1} \odot f_t \\ o_t &= \sigma(x_t * w_{xo} + h_{t-1} * w_{ho} + w_{obias}) \\ h_t &= o_t \odot \tanh(c_t) \end{cases} \quad (1)$$

where x_t represents the input at time t , *i.e.* the feature maps of the frame t ; i_t , f_t , \tilde{c}_t , and o_t represent the input, forget, cell, and output gates, respectively; c_t , c_{t-1} , h_t , and h_{t-1} are the memory and output activations at time t and $t-1$, respectively; σ and \tanh are the sigmoid and hyperbolic tangent non-linearities; $*$ represents the convolution operation, and \odot the Hadamard product. For input feature maps of size $d \times h \times w$, the *LSTM* module outputs a memory map of size $d_m \times h \times w$, where d_m is the number of temporal features learnt by the memory. Note that the recurrent connections operate only over the temporal dimension, and use local convolutions to capture spatial context. We implemented and experimented with spatial recurrent 2D LSTM cells as well, to gain more flexibility in handling spatial context. However, since the recurrent connections require sequential processing, the execution time becomes prohibitive especially during training; therefore we decided to sacrifice the spatial recurrent connections. Note that a similar convolutional LSTM implementation was recently used by Shi et al. (2015) for precipitation nowcasting.

3.2.2 OPTICAL FLOW PREDICTION Θ WITH HUBER PENALTY H

The optical flow prediction module generates a dense transformation map \mathcal{T} , having the same height and width as the memory output, with one 2D flow vector per pixel, representing the displacement in x and y directions due to motion between consecutive frames. \mathcal{T} allows predicting the next frame by warping the current frame. We use two convolutional layers with relatively large kernels (15×15) to regress from the memory feature space to the space of flow vectors. Large kernels are needed since the magnitude of the predicted optical flow is limited by the size of the filters. To ensure local smoothness, we need to penalise the local gradient of the flow map $\nabla \mathcal{T}$. We add a penalty module H whose role is to forward its input unchanged during the forward pass, and to inject non-smoothness error gradient during the backward pass, towards the modules that precede

it in the architecture and that might have contributed to the error. We use Huber loss as penalty (2) with its corresponding derivative (3), due to its edge-preserving capability (Werlberger et al., 2009). The gradient of the flow map is obtained by convolving the map with a fixed (non-trainable) $2 \times 3 \times 3$ filter, corresponding to a 5-point stencil, and 0 bias.

$$\mathcal{H}_\delta(a_{ij}) = \begin{cases} \frac{1}{2}a_{ij}^2, & \text{for } |a_{ij}| \leq \delta, \\ \delta(|a_{ij}| - \frac{1}{2}\delta), & \text{otherwise,} \end{cases} \quad (2)$$

$$\nabla \mathcal{H}_\delta(a_{ij}) = \begin{cases} a_{ij}, & \text{for } |a_{ij}| \leq \delta, \\ \delta \text{sign}(a_{ij}), & \text{otherwise.} \end{cases} \quad (3)$$

Here, a_{ij} represent the elements of $\nabla \mathcal{T}$. In our experiments, we used $\delta = 10^{-3}$.

3.2.3 GRID GENERATOR GG AND IMAGE SAMPLER S

The grid generator GG and the image sampler S output the predicted feature maps \tilde{x}_{t+1} of the next frame after warping the current feature maps x_t with the flow map produced by the Θ module. We use similar differentiable grid generator and image sampler as STN (Jaderberg et al., 2015). The output of S , of size $d \times h \times w$, is considered as a fixed $h \times w$ grid, holding at each (x_o, y_o) position a feature map entry of size $1 \times 1 \times d$. We modified the grid generator to accept one transformation per pixel, instead of a single transformation for the entire image as in STN. Given the flow map \mathcal{T} , GG computes for each element in the grid the source position (x_s, y_s) in the input feature map from where S needs to sample to fill in the position (x_o, y_o) :

$$\begin{pmatrix} x_s \\ y_s \end{pmatrix} = \mathcal{T}(x_o, y_o) \begin{pmatrix} x_o \\ y_o \\ 1 \end{pmatrix}, \mathcal{T}(\cdot, \cdot) = \begin{pmatrix} 1 & 0 & t_x \\ 0 & 1 & t_y \end{pmatrix}. \quad (4)$$

The Θ module outputs two parameters (t_x, t_y) for each pixel. The forward pass of GG is given by equation (4). In the backward pass, GG simply backpropagates the derivative of equation (4) w.r.t. the input parameters (t_x, t_y) .

3.2.4 LOSS FUNCTION

Training the network comes down to minimising the reconstruction error between the predicted next frame and the ground truth next frame, under specific constraints. To enforce edge preservation, we quantify the reconstruction error through a loss function similar to (Eigen & Fergus, 2015). Namely, we consider the error between the gradients of the predicted next frame and the ground truth next frame. Additionally, as mentioned before, we inject Huber penalty gradient during backpropagation on the optical flow map. We do not apply any preprocessing step to the input images (subtracting mean, or local contrast normalisation), since this would discard the low frequencies, which we believe are important for motion estimation. Hence, the overall objective to minimise is given by:

$$\mathcal{L}_t = \|\nabla \tilde{Y}_{t+1} - \nabla Y_{t+1}\|^2 + w_H \mathcal{H}(\nabla \mathcal{T}), \quad (5)$$

where w_H is a hard-coded parameter used to weight the smoothness constraints w.r.t. the data term; in our experiments $w_H = 10^{-2}$.

3.3 NETWORK PARAMETERS

The whole network has 703,651 trainable parameters distributed as described in Table 1. The spatial encoder and decoder have 32 filters each, size 7×7 . The memory module ($LSTM$) has 45 filters, size 7×7 , and the optical flow regressor Θ has 2 convolutional layers, each with 2 filters of size 15×15 , and a 1×1 convolutional layer. The other modules: GG , H , and S have no trainable parameters.

4 TRAINING

To train the proposed architecture, we follow a setup similar to (Stollenga et al., 2015); we use *rmsprop*, with parameters $\epsilon = 10^{-5}$, $\rho = 0.9$, and a decaying learning rate following the rule

Module	Number of trainable parameters
Spatial encoder (E)	1,600
Spatial decoder (D)	1,569
Memory ($LSTM$)	679,320
Optical flow regressor (Θ)	21,162
Total	703,651

Table 1: Network parameters per module.

$\eta = 10^{-4} \left(100 \sqrt{\frac{1}{2}} \right)^{\text{epoch}}$. The biases of the forget gates are initialised to 1; for the other gates we set the biases to 0. The training data is represented by multiple gray-scale video sequences. At each time step, we sample a subsequence of τ consecutive frames, and the goal is to reconstruct the next frame, $(\tau + 1)^{\text{th}}$, in the sequence. Therefore, the network is unfolded over τ steps (as illustrated in Figure 2). After processing the subsequence, we update the parameters and we reset the memory. The initialisation of all the convolutional layers except those involved in the memory module was done using *xavier* method (Glorot & Bengio, 2010). During training, before each parameter update, we clip the gradients to lie in a predefined range, to avoid numerical issues (Graves, 2013).

Our implementation is based on Torch library (Collobert et al.) and extends the *rnn* package. All our code is available online (Con). The training was done on an 880M Nvidia GPU (8G of GPU memory).

5 EXPERIMENTS

We ran experiments on synthetic and real datasets, to debug the individual modules composing the architecture and to assess the overall behaviour. We present only preliminary qualitative results. We are currently working on generating an appropriate dataset that would allow a quantitative evaluation of our system, namely videos with ground truth optical flow maps. Existing datasets in the optical flow community contain flow maps for pairs of images only (Fischer et al., 2015), not for video sequences. Sintel dataset (Butler et al., 2012) contains indeed ground truth optical flow for video sequences. However, it exhibits a complex combination of camera self-motion and moving objects, with a relatively low frame rate, leading to very large (non-realistic) displacements between consecutive frames. Note also that the self-motion makes the entire scene to *move* in terms of optical flow, making the prediction very hard and, in the same time, not useful for the purposes of our work: if all the points in the scene move, it is difficult to delineate objects. Instead, we used this dataset to confirm the ability of the grid generator GG and image sampler S to generate the next frame given the current frame and the correct optical flow map, by isolating the two modules from the rest of the architecture. Figure 3 shows an example of warping. Note that since the flow displacement is significant in this dataset, the sampling result can contain artifacts, especially near boundaries, caused by occlusions. The average error induced by the sampler on this dataset is of 0.004. However, this test was done by sampling directly from the input frames, no spatial encoder – decoder was used. In our architecture, these artifacts will be washed out to a certain extent by the convolutional decoder. The optical flow throughout this section is displayed using the colour code from (Baker et al., 2011), illustrated in Figure 4.

The training of the overall architecture was done using moving MNIST dataset (Srivastava et al., 2015), and a dataset of real video sequences extracted from PROST (Santner et al., 2010) and ViSOR (Vezzani & Cucchiara, 2010) datasets; see Figure 5 for sample images.

MOVING MNIST

Moving MNIST dataset consists of 10k sequences of 20 frames each, obtained by moving (translating) MNIST digit images inside a square of size 64×64 , using uniform random sampling to obtain direction and velocity; the sequences can contain several overlapping digits in one frame. We ran experiments on the original dataset and on a modified version of it, in which we superimposed a pair of lines, one vertical and one horizontal, at random positions, to act as fixed reference in understanding the digits’ movement.



Figure 3: Warping performed by the *GG* and *S* modules, given a video frame and the ground truth optical flow map. First line: input frame and ground truth optical flow map displayed using the colour code shown in Figure 4. Second line: ground truth next frame and sampled next frame; note the artifacts close to the boundaries.

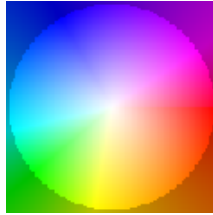


Figure 4: Colour code used to display the optical flow (Baker et al., 2011); the colour encodes the direction of movement and the colour intensity reflects the magnitude; darker shades correspond to higher magnitudes.

Figure 6 shows representative qualitative results obtained on moving MNIST dataset and on the modified version. The slightly cleaner optical flow in the experiment with lines could suggest that it is important to have static image elements when trying to understand moving elements. Overall, these preliminary results are very encouraging and show that the network captures the movement and generates accurate predictions for the next frame in the sequence, even when overlaps or bouncing against the limits of the squares occur. The lines in the modified moving MNIST can help the reader to see clearly that the objects are translated in the correct positions in the predicted next frame. Equally, these results show that the optical flow maps produced by the network correspond to a basic form of image segmentation into objects identified by their movement. Due to the built-in feedback loop, no labelled data is needed. Hence, this setup could potentially be more useful to pre-train a network for supervised video segmentation than a classic video autoencoder.

REAL DATASET

The real dataset consists of 11 video sequences extracted from PROST and ViSOR, with 11027 frames in total, size 160×120 . The videos are taken by non-moving cameras and contain moving objects in scenes with relatively cluttered background. Moreover, they can contain articulated objects in which parts can have different local motion, and scenes with occluding elements. Figure 7 shows qualitative results on different sequences from the dataset. The optical flow maps indicate clearly that the moving elements of the scene are identified by the network, even in scenes with cluttered background. Note that the optical flow maps have cleaner background compared to the moving MNIST experiment, owing to the visibly static elements in the background.



Figure 5: Samples of images from moving MNIST and PROST datasets.



Figure 6: Qualitative results on moving MNIST dataset (left) and moving MNIST with lines (right). In both cases, the first five columns show the last frames fed into the network (from $t - 4$ to t), the $t + 1$ column shows the ground truth next frame, and the last two columns show the predicted next frame and the predicted optical flow.

6 CONCLUSION AND FUTURE WORK

We proposed an original spatio-temporal video autoencoder based on an end-to-end differentiable architecture that allows unsupervised training for motion prediction. The core of the architecture is a module implementing a convolutional version of long short-term memory (LSTM) cells to be used as a form of artificial visual short-term memory. The immediate next step is to incorporate the pre-trained spatial and memory modules within a supervised setup targeting a high-level task,

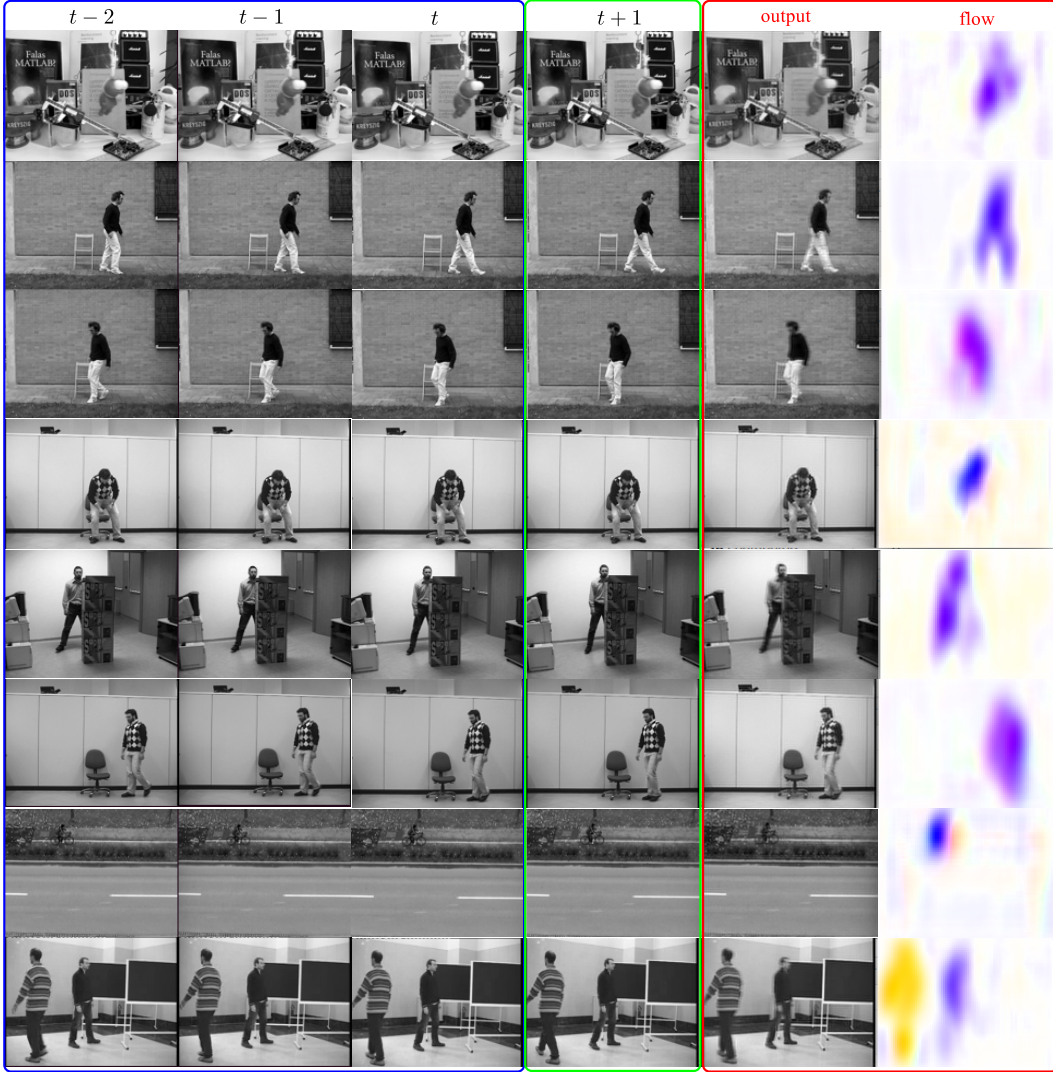


Figure 7: Qualitative results on real videos. The first three columns show the last frames fed into the network (from $t - 2$ to t), the $t + 1$ column shows the ground truth next frame, and the last two columns show the predicted next frame and the predicted optical flow.

e.g. semantic segmentation. The proposed architecture is a proof-of-concept, and possibly its performance would improve by making the whole architecture deeper.

On a more general note, we believe that our work can open up the path to a number of exciting directions. Due to the built-in feedback loop, various experiments can be carried out effortlessly, to develop further the basic memory module that we proposed. In particular, investigating on the size of the memory and its resolution/downsampling could shed some light into the causes of some geometric optical illusions; *e.g.* when storing in memory an overly-downsampled version of the visual input, this could affect the capacity of correctly perceiving the visual stimuli, in accordance with Shannon-Nyquist sampling theorem (Shannon, 1949). Equally, we hypothesise that our convolutional version of LSTM cells can lead to ambiguous memory activations, *i.e.* the same activation would be produced when presenting a temporally moving boundary or a spatially repeated boundary. This could imitate the illusory motion experienced by biological VSTMs, *i.e.* static repeated patterns that produce a false perception of movement (Conway et al., 2005).

In the current implementation the cells’ layout follows the input’s layout, and all the weights are shared, meaning that the entire content is represented at the same resolution. However, neuroscience

studies suggest that this is not the case for biological memories, hence experiments with non-shared weights to allow different resolutions depending on the spatial distribution could be carried out. Last but not least, the proposed architecture composed of memory module and built-in feedback loop could be applied for static images as a compression mechanism, in an attempt to train an iconic memory, similar to the inspirational work on jigsaw video compression (Kannan et al., 2007). The memory addressing in that case could use a content-based mechanism similar to NTM (Graves et al., 2014).

ACKNOWLEDGMENTS

We are greatly indebted to the *Torch* community for their efforts to maintain this great library, and we are grateful to CSIC Cambridge for funding this work.

REFERENCES

- ConvLstm. <https://github.com/viorik/ConvLSTM>.
- Agrawal, Pulkit, Carreira, João, and Malik, Jitendra. Learning to see by moving. *CoRR*, abs/1505.01596, 2015. URL <http://arxiv.org/abs/1505.01596>.
- Alexe, B., Deselaers, T., and Ferrari, V. Measuring the objectness of image windows. *IEEE Trans. Pattern Anal. Mach. Intell.*, 34(11), 2012. doi: 10.3758/BF03203943.
- Baillargeon, René. Infants’ physical world. *American Psychological Society*, 13(3), 2004.
- Baker, Simon, Scharstein, Daniel, Lewis, J. P., Roth, Stefan, Black, Michael J., and Szeliski, Richard. A database and evaluation methodology for optical flow. *Int. J. Comput. Vision*, 92(1):1–31, 2011.
- Boahen, K. Neuromorphic microchips. *Scientific American*, 292(5), 2005.
- Butler, D. J., Wulff, J., Stanley, G. B., and Black, M. J. A naturalistic open source movie for optical flow evaluation. In *European Conf. on Computer Vision (ECCV)*, pp. 611–625, 2012.
- Collobert, Ronan, Kavukcuoglu, Koray, and Farabet, Clément. Torch7: A matlab-like environment for machine learning.
- Conway, Bevil R., Kitaoka, Akiyoshi, Yazdanbakhsh, Arash, Pack, Christopher C., and Livingstone, Margaret S. Neural basis for a powerful static motion illusion. *The Journal of Neuroscience*, 25(23):5651–5656, 2005.
- Eck, Douglas and Schmidhuber, Jürgen. A first look at music composition using lstm recurrent neural networks. Technical Report IDSIA-07-02, IDSIA / USI-SUPSI.
- Eigen, David and Fergus, Rob. Predicting depth, surface normals and semantic labels with a common multi-scale convolutional architecture. In *ICCV*, 2015.
- Fischer, Philipp, Dosovitskiy, Alexey, Ilg, Eddy, Häusser, Philip, Hazirbas, Caner, Golkov, Vladimir, van der Smagt, Patrick, Cremers, Daniel, and Brox, Thomas. FlowNet: Learning optical flow with convolutional networks. *CoRR*, abs/1504.06852, 2015. URL <http://arxiv.org/abs/1504.06852>.
- Geiger, Andreas, Lenz, Philip, and Urtasun, Raquel. Are we ready for autonomous driving? the kitti vision benchmark suite. In *Conference on Computer Vision and Pattern Recognition (CVPR)*, 2012.
- Glorot, Xavier and Bengio, Yoshua. Understanding the difficulty of training deep feedforward neural networks. In *AISTATS*, 2010.
- Graves, Alex. Generating sequences with recurrent neural networks. *CoRR*, abs/1308.0850, 2013.
- Graves, Alex, Fernández, Santiago, and Schmidhuber, Jürgen. Multi-dimensional recurrent neural networks. In *Artificial Neural Networks*, volume 4668, pp. 549–558. 2007.

- Graves, Alex, Wayne, Greg, and Danihelka, Ivo. Neural turing machines. *CoRR*, abs/1410.5401, 2014.
- Hochreiter, Sepp and Schmidhuber, Jürgen. Long short-term memory. *Neural Comput.*, 9(8):1735–1780, November 1997. ISSN 0899-7667. doi: 10.1162/neco.1997.9.8.1735. URL <http://dx.doi.org/10.1162/neco.1997.9.8.1735>.
- Hochreiter, Sepp, Informatik, Fakultät F., Bengio, Yoshua, Frasconi, Paolo, and Schmidhuber, Jürgen. Gradient Flow in Recurrent Nets: the Difficulty of Learning Long-Term Dependencies. In *Field Guide to Dynamical Recurrent Networks*. 2000.
- Hollingworth, A. Constructing visual representations of natural scenes: the roles of short- and long-term visual memory. *J Exp Psychol Hum Percept Perform.*, 30(3), 2004.
- Horn, Berthold K. P. and Schunck, B. G. Artificial intelligence in perspective. chapter Determining Optical Flow: A Retrospective, pp. 81–87. 1994.
- Jaderberg, Max, Simonyan, Karen, Zisserman, Andrew, and Kavukcuoglu, Koray. Spatial transformer networks. *CoRR*, abs/1506.02025, 2015. URL <http://arxiv.org/abs/1506.02025>.
- Kannan, Anitha, Winn, John, and Rother, Carsten. Clustering appearance and shape by learning jigsaws. In *Advances in Neural Information Processing Systems*, pp. 657–664. 2007.
- Kim, Hanme, Handa, Ankur, Benosman, Ryad, Ieng, Sio-Hoi, and Davison, Andrew J. Simultaneous mosaicing and tracking with an event camera. In *British Machine Vision Conference (BMVC)*. BMVC 2014, 2014.
- Magnussen, Svein. Low-level memory processes in vision. *Trends in Neurosciences*, 23(6):247–251, 2000. ISSN 0166-2236. doi: [http://dx.doi.org/10.1016/S0166-2236\(00\)01569-1](http://dx.doi.org/10.1016/S0166-2236(00)01569-1). URL <http://www.sciencedirect.com/science/article/pii/S0166223600015691>.
- Masci, Jonathan, Meier, Ueli, Cirean, Dan, and Schmidhuber, Jürgen. Stacked convolutional auto-encoders for hierarchical feature extraction. In *Artificial Neural Networks and Machine Learning*, volume 6791, pp. 52–59. 2011.
- Menze, Moritz and Geiger, Andreas. Object scene flow for autonomous vehicles. In *Proceedings of the IEEE Conference on Computer Vision and Pattern Recognition*, pp. 3061–3070, 2015.
- Phillips, W.A. On the distinction between sensory storage and short-term visual memory. *Perception & Psychophysics*, 16(2):283–290, 1974. ISSN 0031-5117. doi: 10.3758/BF03203943. URL <http://dx.doi.org/10.3758/BF03203943>.
- Sak, Hasim, Senior, Andrew W., and Beaufays, Françoise. Long short-term memory based recurrent neural network architectures for large vocabulary speech recognition. *CoRR*, abs/1402.1128, 2014. URL <http://arxiv.org/abs/1402.1128>.
- Santner, Jakob, Leistner, Christian, Saffari, Amir, Pock, Thomas, and Bischof, Horst. PROST Parallel Robust Online Simple Tracking. In *IEEE Computer Society Conference on Computer Vision and Pattern Recognition (CVPR)*, San Francisco, CA, USA, 2010.
- Shannon, C.E. Communication in the presence of noise. *Proceedings of the IRE*, 37(1):10–21, Jan 1949. ISSN 0096-8390. doi: 10.1109/JRPROC.1949.232969.
- Shi, Xingjian, Chen, Zhourong, Wang, Hao, Yeung, Dit-Yan, Wong, Wai-Kin, and Woo, Wang-chun. Convolutional LSTM network: A machine learning approach for precipitation nowcasting. *CoRR*, abs/1506.04214, 2015.
- Srivastava, Nitish, Mansimov, Elman, and Salakhutdinov, Ruslan. Unsupervised learning of video representations using lstms. *ICML*, 2015.
- Stollenga, Marijn, Byeon, Wonmin, Liwicki, Marcus, and Schmidhuber, Jürgen. Parallel multi-dimensional lstm, with application to fast biomedical volumetric image segmentation. *CoRR*, abs/1506.07452, 2015. URL <http://arxiv.org/abs/1506.07452>.

- Sutskever, Ilya, Vinyals, Oriol, and Le, Quoc V. Sequence to sequence learning with neural networks. *NIPS*, 2014.
- Vezzani, Roberto and Cucchiara, Rita. Video surveillance online repository (visor): an integrated framework. *Multimedia Tools and Applications*, 50(2):359–380, 2010.
- Weinzaepfel, P., Revaud, J., Harchaoui, Z., and Schmid, C. Deepflow: Large displacement optical flow with deep matching. In *Computer Vision (ICCV), 2013 IEEE International Conference on*, pp. 1385–1392, Dec 2013. doi: 10.1109/ICCV.2013.175.
- Werlberger, Manuel, Trobin, Werner, Pock, Thomas, Wedel, Andreas, Cremers, Daniel, and Bischof, Horst. Anisotropic Huber-L1 optical flow. In *Proceedings of the British Machine Vision Conference (BMVC)*, London, UK, September 2009.
- Williams, Ronald J. and Zipser, David. Backpropagation. chapter Gradient-based Learning Algorithms for Recurrent Networks and Their Computational Complexity, pp. 433–486. 1995.